Biological Procedures Online

RESEARCH Open Access

Chang-Wei-Qing Combined with PD-1 Inhibitor Alleviates Colitis-Associated Colorectal Tumorigenesis by Modulating the Gut Microbiota and Restoring Intestinal Barrier

Junkai Wen[1†], Shunyun Wang[1†], Kexiang Sun[1], Haoyue Wang[1], Zeting Yuan[2*] and Wanli Deng[1*]

Abstract

Chang-Wei-Qing (CWQ) is a widely recognized Traditional Chinese Medicine (TCM) formulation composed of *Astragalus*, *Codonopsis*, *Atractylodes*, *Poria*, *Coix* seed, *Akebia trifoliata Koidz*, *Sargentodoxa cuneata*, and *Vitis quinquangularis Rehd*. This formulation has garnered significant interest for its positive effects in mitigating colorectal cancer, and when combined with PD-1, it affects some gut microbiota associated with tumor infiltrating lymphocytes cells. However, the biological rationale underlying the suppression of colitis-associated colorectal cancer (CAC) in AOM/DSS-treated mice by CWQ combined with PD-1 inhibitor remains to be explored. Our aim is to explore the chemopreventive effect of CWQ combined with PD-1 inhibitor on CAC, with a focus on modulating the gut microbiota. A mouse model of CAC was established using azoxymethane (AOM) and dextran sulfate sodium (DSS) treatment. Pathological evaluation of tissue samples included immunohistochemistry and hematoxylin and eosin staining. Intestinal barrier function was assessed by transmission electron microscopy. Fecal microbiota and metabolites were analyzed through 16 S rRNA gene sequencing and liquid chromatography-mass spectrometry, respectively. Mice treated with antibiotics served as models for fecal microbiota transplantation. CWQ combined with PD-1 inhibitor suppressed CAC in AOM/DSS-treated mice. This combined therapy effectively alleviated gut dysbiosis in the CAC model by increasing microbial diversity, enriching probiotic populations such as *Limosilactobacillus* and *Bifidobacterium*, and reducing pathogenic bacteria like *Desulfovibrio*. Additionally, CWQ combined with PD-1 inhibitor downregulated metabolites associated with the *NF-kappa B signaling pathway*. The combined treatment also significantly improved intestinal barrier function in CAC mice. Transmission electron microscopy of the CWQ combined with PD-1 inhibitor group showed enhanced cellular integrity, a relatively

[†]Junkai Wen and Shunyun Wang contributed equally to this work.

*Correspondence:
Zeting Yuan
yuan340202@163.com
Wanli Deng
tcmdwl@163.com

Full list of author information is available at the end of the article

normal mitochondrial structure with intact membranes, and a more abundant, unexpanded endoplasmic reticulum, underscoring the protective effects of this combination on intestinal barrier integrity. Transcriptomic analysis further demonstrated that the combined therapy upregulated genes involved in tight and adherens junctions, while downregulating genes linked to innate immune responses. CWQ combined with PD-1 inhibitor can ameliorate dysbiosis in the AOM/DSS mouse model, with the metabolites of the gut microbiome potentially possessing anti-inflammatory activity. Moreover, CWQ combined with PD-1 inhibitor improves intestinal barrier function, thereby effectively inhibiting the occurrence and development of CAC.

Keywords Colitis-associated colorectal cancer, Chang-Wei-Qing, PD-1 inhibitor, Microbiota, Metabolites

Introduction

Globally, colorectal cancer (CRC) ranks third in terms of frequency of diagnosis among cancers and stands as the second most significant contributor to cancer-related deaths [1, 2]. Apart from genetic factors, chronic inflammation is also a driving force for tumor progression, as evidenced by studies demonstrating a notable rise in CRC risk among individuals with inflammatory bowel disease [3]. PD-1 inhibitors are widely used immunotherapeutic agents of various cancers [4, 5]. However, the efficacy of PD-1 inhibitors in the clinical application of CRC is not stable and shows some side effects [6, 7]. The gut microbiota can influence tumor initiation and progression by affecting immune responses [8–10], while the interaction between microbiota and immune cells is also vital in maintaining intestinal balance and immune microenvironment stability [11, 12]. Studies indicate that altering the composition of gut microbiota can alleviate the progression of inflammation and carcinogenesis, particularly in colitis-associated colorectal cancer (CAC) [13, 14].

Recent findings suggest that Traditional Chinese Medicine (TCM) may influence gut microbiota and metabolites, providing a foundation for their advantageous effects [15, 16]. Chang-Wei-Qing (CWQ) is a widely recognized TCM formulation that has garnered significant interest for its positive effects in mitigating colorectal cancer. It is composed of *Astragalus*, *Codonopsis*, *Atractylodes*, *Poria*, *Coix* seed, *Akebia trifoliata Koidz*, *Sargentodoxa cuneata*, and *Vitis quinquangularis Rehd*. Recently, CWQ has been demonstrated to increase the tumor infiltration of CD3+and CD8+T cells, and when combined with PD-1, it affects some gut microbiota associated with tumor infiltrating lymphocytes cells [17]. However, the biological rationale underlying the suppression of CAC in mice treated with azoxymethane/dextran sulfate sodium (AOM/DSS) by CWQ in combination with PD-1 inhibitor remains to be elucidated.

Hence, we systematically demonstrated that the CWQ combined with PD-1 inhibitor suppressed colitis-associated colorectal tumorigenesis in AOM/DSS mice models (Fig. 1), highlighting the potential for transforming gut microbiota knowledge into clinical practice solutions. Utilizing TCM formulations as adjuncts to chemotherapy and immunotherapy, we strived to enhance drug efficacy and safety. Our ultimate goal was to develop targeted microbiota therapies for optimizing the utilization of the gut microbiota. Our findings indicated that this combination treatment could reverse gut dysbiosis associated with CAC by enriching probiotics, while improving intestinal barrier function in CAC. Furthermore, we conducted assessments on the chemopreventive effectiveness of CWQ combined with PD-1 inhibitor in CAC, using antibiotic-treated mice as part of our investigation. Together, we proposed that the antitumor efficacy of this combination therapy in CAC was attributed to its impact on the gut microbiota and intestinal barrier, which had been thoroughly studied experimentally to elucidate specific mechanisms. These findings were aimed at offering new perspectives and insights for the development of combined treatments targeting CAC.

Materials and Methods

Reagents

Azoxymethane (AOM, A2853), dextran sulfate sodium (DSS), sodium carboxymethyl cellulose, citrate antigen retrieval solution (pH 6.0), paraffin (Leica Camera AG), anti-Ki67 antibody (ab15580, Abcam, USA), anti-ZO-1 (Abcam, USA), mouse anti-Occludin (CST, USA), and anti-Claudin (Abcam, USA), GSM-TH17 assay kit (RayBiotech), methanol (HPLC), acetonitrile (HPLC), formic acid (HPLC), 2-propanol, and 2-Chloro-L-Phenylalanine (≥98%).

Mouse Models of CAC and Combined Treatment with CWQ and PD-1 Inhibitor

Specific-pathogen-free female C57BL/6 mice (5 weeks old, 17.0±3.0 g, n=30) were procured from Shanghai SLAC Laboratory Animal Co., acclimatized for a week, and then intraperitoneally injected with 12.5 mg/kg AOM to induce tumorigenesis. Subsequently, they underwent three cycles of DSS treatment to mimic CAC. Throughout each cycle, the mice were provided unrestricted access to drinking water containing 2.5% DSS for 7 days, followed by a subsequent 14-day period of regular water consumption (Fig. 2A).

The mice were randomly divided into four groups (n=6 per group): the control group (received 0.2 mL normal

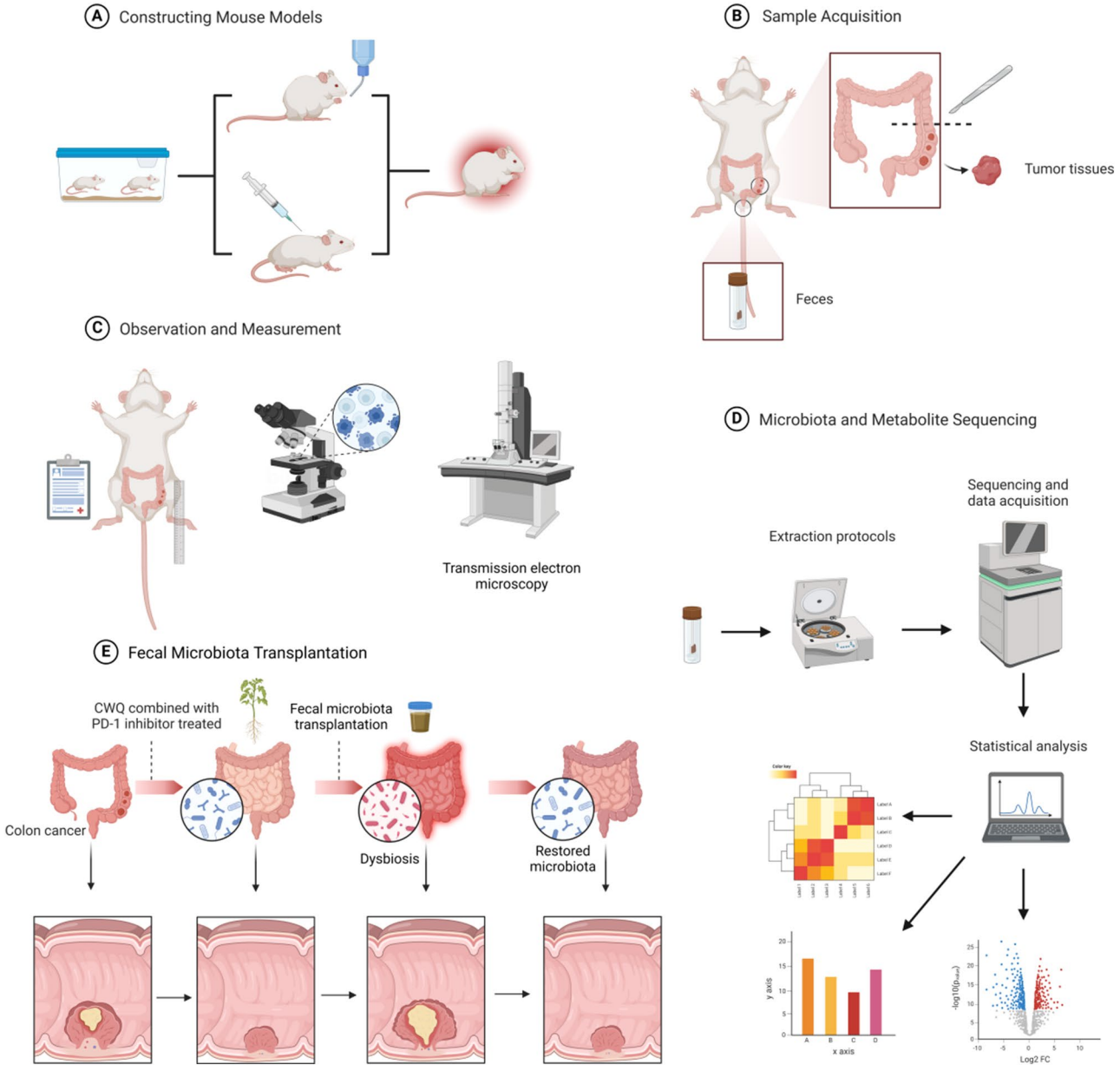

Fig. 1 Experimental Workflow Overview. (**A**) AOM/DSS treatment was administered initially to establish the CAC mouse model. (**B**) Following the successful establishment of the model, tumor tissues and fecal samples were collected from the mice. (**C**) Tumor tissues underwent pathological examination, and intestinal barrier function was assessed using transmission electron microscopy. (**D**) Fecal microbiota and metabolites were analyzed using 16 S rRNA gene sequencing and liquid chromatography-mass spectrometry, respectively. (**E**) The impact of intestinal microbiota on CAC was verified through fecal microbiota transplantation

saline i.g. and 0.1 mL normal saline i.v.), the CWQ group (received 0.2 mL CWQ i.g. and 0.1 mL normal saline i.v.), the PD-1 inhibitor group (received 0.1 mL of the PD-1 inhibitor i.v. and 0.2 mL normal saline i.g.), and the CWQ combined with PD-1 inhibitor group (received 0.2 mL CWQ i.g. and 0.1 mL of the PD-1 inhibitor i.v.).

CWQ was administered orally at a dose of 25.74 g/kg daily following AOM injection until the study endpoint, while the PD-1 inhibitor was given once every four days. The dosage of 25.74 g/kg was determined based on clinical prescription dosages for humans (198 g/70kg), taking into account the body surface area adjustment between humans and animals (198 g/70kg × 9.1 ≈ 25.74 g/kg).

The mice were euthanized at week 18 post the initial AOM injection, in accordance with the approved experimental protocol by the Animal Experimentation Ethics Committee of Shanghai University of TCM (approval number: DWEC-A-202206012).

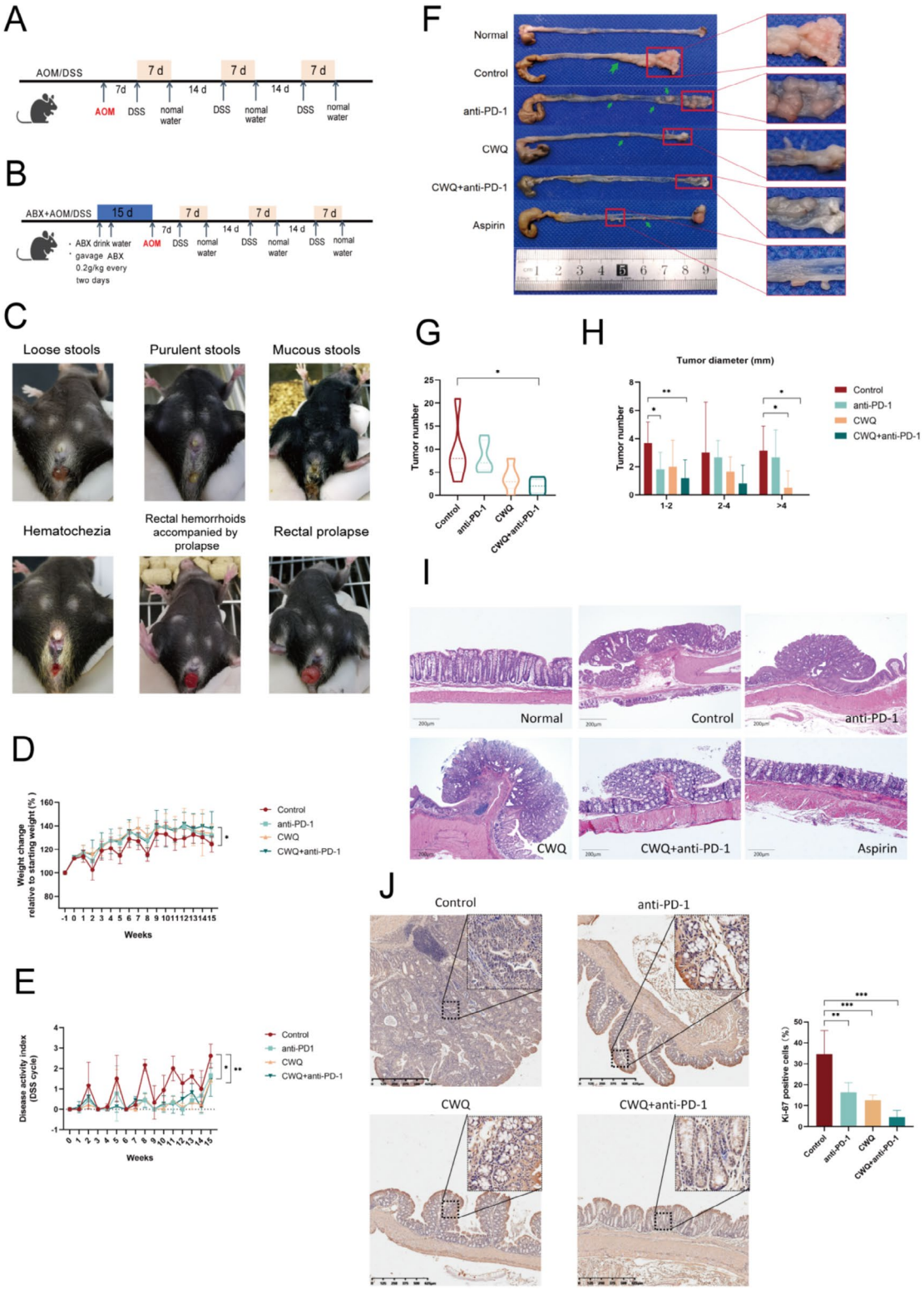

Fig. 2 CWQ combined with PD-1 inhibitor suppresses CAC in AOM/DSS-treated mice. (**A**) Establishment of CAC model in C57BL/6 mice. (**B**) Establishment of antibiotic-treated mouse model. (**C**) Effects of AOM/DSS treatment on colitis symptoms in mice. (**D**) Changes in body weight of mice in different groups. (**E**) Changes in DAI of mice in different groups during the DSS cycle. (**F**) The manifestations of the colonic tissues and tumor tissues of mice after different interventions. (**G**) The number of tumors in mice after different interventions. (**H**) The diameter of tumors in mice after different interventions. (**I**) The manifestations of H&E staining in the colonic mucosal tissues of mice after different interventions. (**J**) The expression of Ki-67 in the tumor tissues of mice after different interventions. *$P < 0.05$, **$P < 0.01$ and ***$P < 0.001$

Antibiotic-Treated Mice

Specific-pathogen-free female C57BL/6 mice (5 weeks old, weighing 17.0±3.0 g, $n=24$) were adaptively fed for a week after purchase. Their normal drinking water was then replaced with an ABX antibiotic mixed solution (1 g/L ampicillin, 1 g/L neomycin, 1 g/L metronidazole, 0.5 g/L vancomycin) for a period of 15 days (Fig. 2B). Mice weighing more than 16 g were selected, and the remaining steps were the same as those for the AOM/DSS-treated mice.

Fecal Microbiota Transplantation to Antibiotic-Treated Mice

Fecal samples were collected from donor mice on day 15, following a 14-day period of drug intervention. Fresh fecal samples were processed and the microbial suspension prepared within 24 h of collection. Twenty mice that met the weight criteria were randomly allocated into four groups ($n=5$ per group). Each group received daily gavage with fecal samples from the control group, CWQ group, PD-1 inhibitor group, and CWQ combined with PD-1 inhibitor treated mice, respectively. Briefly, 1 g of stool samples was homogenized in 6.5 mL of PBS, and 200 μL of the suspension was gavaged per mouse. Subsequent procedures were carried out as outlined for conventional mice.

Drug Preparation

CWQ consists of 30 g *Astragalus*, 15 g *Codonopsis*, 15 g *Atractylodes*, 24 g *Poria*, 30 g *Coix* seed, 24 g *Akebia trifoliata Koidz*, 30 g *Sargentodoxa cuneata*, and 30 g *Vitis quinquangularis Rehd*. The eight herbal drugs' doses were converted into granules at Tianjiang Pharmaceutical Co. Ltd. (Jiangyin, China), and dissolved in distilled water to achieve a concentration of 2.574 g/mL. These decoctions were stored at 4 °C. Additionally, the PD-1 inhibitor, procured from Xinda Biopharmaceutical Co. Ltd. (Suzhou, China), was dissolved in PBS to a concentration of 0.5 mg/mL and stored at 4℃.

Aspirin tablets were crushed into a fine powder using a mortar and pestle. A total of 150 mg of the powdered aspirin was accurately weighed using a microbalance and dissolved in 50.0 ml of a 0.5% carboxymethyl cellulose sodium solution, resulting in a 3.0 mg/ml aspirin solution. Each mouse was administered the aspirin solution via gavage at a dose of 0.01 ml per gram of body weight, which corresponds to a final dosage of 30.0 mg/kg.

Histopathology and Immunostaining

The intestinal tissue, positioned 4 cm above the anus, was excised from the mice. Approximately 1 cm of the dissected tissue underwent rinsing with ice-cold saline, fixation in 10% formalin, embedding in paraffin, sectioning, and subsequent staining with hematoxylin-eosin (H&E). Following dehydration via an ethanol gradient and xylene incubation, the samples were mounted for observation under a light microscope (Olympus, Tokyo, Japan).

For immunohistochemistry, the deparaffinized intestinal tissue sections underwent antigen retrieval through heating in 10 mM citrate buffer (pH 9.0) and treatment with 3% hydrogen peroxide. Mouse anti-ZO-1 (Abcam, USA), mouse anti-Occludin (CST, USA), and anti-Claudin (Abcam, USA) antibodies were used at dilutions of 1 : 500, 1 : 200, and 1 : 250, respectively. For Ki-67 immunohistochemistry in tumor tissues, the deparaffinized sections were processed in the same way as above. Anti-Ki-67 antibody (ab15580, Abcam, USA) was diluted and used. Subsequently, corresponding horseradish-peroxidase-conjugated secondary antibodies were applied for each, and the targeted antigens were visualized using 3,3'-diaminobenzidine tetrahydrochloride under a light microscope (Olympus, Tokyo, Japan).

16S rRNA Gene Sequencing of Fecal Bacteria

Fecal samples, obtained post-drug intervention from mice and preserved at -80 °C, underwent 16 S rRNA-gene sequencing. Total RNA extraction from these samples utilized TRIzol® Reagent following the manufacturer's protocol. The RNA quality assessment was conducted using the 5300 Bioanalyzer (Agilent) and quantification was performed using the ND-2000 (NanoDrop Technologies). The V3-V4 hypervariable region of the bacterial 16 S rRNA gene was amplified using primer pairs 338 F and 806R in an ABI GeneAmp® 9700 polymerase chain reaction thermocycler (ABI, CA, USA). PCR conditions comprised an initial denaturation at 95 °C for 3 min, followed by 27 cycles of denaturation at 95 °C for 30 s, annealing at 55 °C for 30 s, extension at 72 °C for 45 s, and a final extension at 72 °C for 10 min, with a final hold at 4 °C. The PCR products were analyzed on a 2% agarose gel, and the corresponding amplicons were extracted using the AxyPrep DNA Gel Extraction Kit (Axygen Biosciences, CA, USA) and quantified using the Quantus™ Fluorometer (Promega, USA). These steps were performed in triplicate.

Subsequently, the purified amplicons were equimolarly pooled and subjected to paired-end sequencing on an Illumina MiSeq PE300 platform/NovaSeq PE250 platform (Illumina, San Diego, USA) by Majorbio Bio-Pharm Technology Co. Ltd. (Shanghai, China) following standard protocols. Operational taxonomic units (OTU) with a 97% similarity cutoff were clustered using UPARSE version 7.1, and chimeric sequences were identified and eliminated. The taxonomic classification of each OTU representative sequence was carried out using RDP Classifier version 2.2 against the 16 S rRNA database (e.g., Silva v138) with a confidence threshold of 0.7.

Metabolomic Profiling and Analysis

The sample (50 mg) underwent homogenization with a 6 mm diameter grinding bead and 400 µL of extraction solution (methanol: water = 4:1 (v/v)) containing 0.02 mg/mL of L-2-chlorophenylalanine internal standard. Homogenization was conducted using the Wonbio-96c frozen tissue grinder for 6 min at -10 °C and 50 Hz, followed by low-temperature ultrasonic extraction for 30 min at 5 °C and 40 kHz. Subsequent to centrifugation (15 min, 4 °C, 13000 g), the supernatant was transferred for LC-MS analysis. A pooled quality control sample was prepared by combining equal volumes of all samples and analyzed periodically (every 5 samples) to ensure analysis stability. LC-MS analysis was carried out using a Thermo UHPLC-Q Exactive system equipped with an ACQUITY HSS T3 column. The mobile phases consisted of 0.1% formic acid in water: acetonitrile (95:5, v/v) (solvent A) and 0.1% formic acid in acetonitrile: isopropanol: water (47.5:47.5, v/v) (solvent B). Positive and negative ion mode separation gradients were applied as specified. Data analysis utilized Progenesis QI software with database searches in HMDB (http://www.hmdb.ca/) and Metlin (https://metlin.scripps.edu/) for metabolite identification.

Transcriptomic Analysis of Tumor mRNA

Total RNA was extracted from tissue samples, with concentration and purity measured by the A260/280 ratio, and integrity checked via gel electrophoresis. Fragmentation of isolated mRNA in fragmentation buffer produced ~ 300 bp fragments, selected by magnetic beads. Following primer addition, reverse transcription generated single-strand cDNA, stabilized to double-strand at high temperatures. For sequencing, 15-cycle PCR amplification and agarose gel recovery of target bands preceded Illumina paired-end sequencing (2×150 bp). DNA from each sample was PCR-amplified for the 16 S rRNA V3-V4 region in triplicate. Purified PCR products underwent adapter ligation, magnetic bead selection to remove self-ligated fragments, and final PCR for library enrichment. High-throughput data underwent quality control, merging, and OTU clustering with UPARSE software, while 16 S functional predictions were analyzed using PICRUSt2.

Transmission Electron Microscopy (TEM) Sample Preparation and Imaging Protocol for Tissue Analysis

Fresh tissue samples are carefully selected to minimize mechanical damage, with sample sizes not exceeding 1 mm^3. The tissues are fixed at 4 °C for 2–4 h in electron microscopy fixative and rinsed three times in 0.1 M phosphate buffer (PB, pH 7.4) for 15 min each. Post-fixation follows with 1% osmium tetroxide in PB at room temperature (20 °C) for 2 h, and the samples are rinsed again in PB. Dehydration is conducted through a graded ethanol series (50-100%) and acetone steps, each lasting 15 min. For infiltration, samples are exposed to acetone:812 resin mixtures in ratios of 1:1 for 2–4 h and 1:2 overnight, followed by pure resin infiltration for 5–8 h. Samples are embedded in pure 812 resin on embedding plates, then polymerized in a 60 °C oven for 48 h. Ultrathin Sects. (60–80 nm) are cut using an ultramicrotome and stained with uranyl acetate and lead citrate, each for 15 min, and dried overnight at room temperature. Observations and image analyses are performed with the transmission electron microscope.

Statistical Analysis

Statistical analysis was performed using SPSS 25.0 (IBM Corp., NY, USA). For normally distributed data, comparisons between two groups were conducted using t-tests, while one-way ANOVA was employed for comparisons involving more than two groups. Non-normally distributed data were assessed using rank-sum tests. The threshold for statistical significance was set at $P < 0.05$. Graphs were generated using GraphPad Prism 8 (GraphPad Software Inc., San Diego, USA).

Analysis of mouse gut microbiota data was executed on the Majorbio Cloud Platform (https://cloud.majorbio.com). Alpha diversity metrics including Chao and Shannon indices were computed using mothur software. Inter-group differences in alpha diversity were evaluated using the Wilcoxon rank-sum test. Principal coordinates analysis based on the Bray-Curtis distance algorithm was employed to assess the similarity of microbial community structures across samples. Additionally, non-parametric tests were utilized to detect significant differences in microbial community structures among sample groups. The linear discriminant analysis Effect Size (LDA > 2, $P < 0.05$) was utilized to pinpoint bacterial taxa with notable differences in abundance at various taxonomic levels.

To identify differential expression genes (DEGs) between samples, transcript expression levels were quantified using the TPM method and RSEM. Differential expression analysis was performed using DESeq2 or DEGseq, with DEGs meeting criteria $|\log2FC| \geq 1$ and FDR ≤ 0.05 (DESeq2) or FDR ≤ 0.001 (DEGseq) considered statistically significant. Functional enrichment analysis was conducted to identify pathways enriched with DEGs at Bonferroni-corrected $P \leq 0.05$, using Goatools and KOBAS.

Metabolic features detected in at least 80% of samples were retained and normalized. Variables with RSD > 30% of QC samples were excluded, and log10 transformation was applied. Principal component analysis and orthogonal partial least squares discriminant analysis were performed using the "ropls" R package, with metabolites having VIP > 1 and $P < 0.05$ considered significant.

Differential metabolites were mapped to biochemical pathways using the KEGG database for enrichment analysis, and pathway analysis was conducted using the Python package "scipy.stats".

Results

CWQ Combined with PD-1 Inhibitor Suppresses CAC in AOM/DSS-Treated Mice

AOM/DSS-treated mice exhibited loose stools after the completion of the first round of 2.5% DSS free drinking. Following the conclusion of the second round, the mice presented with mucous and purulent stools, depicted. After the completion of the third round, the mice displayed varying degrees of hematochezia, rectal hemorrhoids accompanied by prolapse, and severe rectal prolapse (Fig. 2C).

The disease activity index (DAI) encompasses evaluations in three key aspects: body weight loss, alterations in fecal characteristics, and rectal bleeding [18]. These parameters serve as effective indicators capable of gauging the severity of colitis or colorectal cancer in mice. Specifically, weight loss may signify a deterioration in the mice's condition, changes in fecal characteristics may mirror the impact of intestinal inflammation or tumor growth on intestinal function, and rectal bleeding is a direct manifestation of bleeding associated with intestinal inflammation or tumors. During experimental weeks 10 to 15, mice in the control group consistently exhibited notably lower body weights compared to those in the CWQ combined with PD-1 inhibitor group ($P<0.05$) (Fig. 2D). Furthermore, during the third DSS cycle, both the CWQ group and the CWQ combined with PD-1 inhibitor group exhibited markedly lower DAI scores compared to the control group ($P<0.05$) (Fig. 2E).

In the group of mice treated with CWQ combined with PD-1 inhibitor, a reduced number of tumors was observed in the rectum, with only minimal raised mucosal tissue evident at the distal end (Fig. 2F), compared to the control, CWQ alone, and PD-1 inhibitor alone groups. Moreover, tumor counts in this combined treatment group (Fig. 2G) were significantly lower than those observed in the control group. Specifically, in both the 1–2 mm and greater than 4 mm tumor size categories, the group treated with CWQ combined with PD-1 inhibitor showed a markedly lower tumor count compared to the control group (Fig. 2H).

The colonic mucosal epithelium in the control group mice is discontinuous, with disrupted glands, edema or disappearance of crypts, extensive infiltration of inflammatory cells, submucosal edema, noticeable rupture and atrophy of villi. Concurrently, the growth and spread of tumors can be clearly observed. In the CWQ combined with PD-1 inhibitor group, a tumor protrusion is observed, but the intestinal villi structure is intact, with closely arranged goblet cells, and the lamina propria shows the distribution of capillaries and scattered lymphocytes (Fig. 2I). We investigated a significant reduction in Ki-67 positive staining granules in the intestines and tumor tissues of mice in the CWQ combined with PD-1 inhibitor group compared to the other groups. Furthermore, the villi were closely arranged, and no apparent tumor-like tissue was observed (Fig. 2J). Conclusively, these results indicated that CWQ combined with PD-1 inhibitor has an inhibitory effect on the growth of CAC cells in AOM/DSS-treated mice.

CWQ Combined with PD-1 Inhibitor Restores Gut Dysbiosis in CAC

To investigate the impact of CWQ combined with PD-1 inhibitor on gut microbiota during colitis-associated colorectal tumorigenesis, we conducted 16 S rRNA-gene sequencing analyses of fecal samples from four groups.

Our alpha diversity analysis, encompassing the ace index, shannon index, and sobs index, demonstrated a notable enhancement in the richness and diversity of gut microbiota with the administration of CWQ combined with PD-1 inhibitor (Fig. 3A). Beta diversity analysis utilizing principal coordinates analysis (PCoA) illustrated a distinct alteration in gut microbiota composition induced by CWQ combined with PD-1 inhibitor (Fig. 3B). Rarefaction and shannon curves derived from the sobs index and shannon index, respectively, indicated sufficient sequencing data depth and sample size (Fig. 3C).

OTU analysis, a commonly used method for characterizing microbial diversity, grouped microbiota with similar sequences into the same OTU. The quantity of OTU served as a crucial metric for evaluating microbial diversity and population levels. Compared to the control group, the other three groups showed varying degrees of OTU elevation, with CWQ combined with PD-1 inhibitor displaying a significant additional enhancement of this indicator (Fig. 3D). Following the administration of CWQ combined with PD-1 inhibitor, a substantial modulation in gut microbiota composition occurred. The relative abundance of bacterial species at the genus level was calculated, and the results are illustrated in Fig. 3E and F. In the AOM/DSS model, probiotics *Limosilactobacillus* [19] and *Bifidobacterium* [20, 21] were enriched by CWQ combined with PD-1 inhibitor, accompanied by a depletion of pathogenic bacteria *Desulfovibrio* [22]. In comparison to the other three groups, CWQ combined with PD-1 inhibitor modulated multiple dysbiotic bacterial species in the CAC group treated with non-CWQ combined with PD-1 inhibitor in the AOM/DSS model. This modulation was evident in the increased abundance of various bacterial genera, suggesting that CWQ combined with PD-1 inhibitor might have a regulatory effect

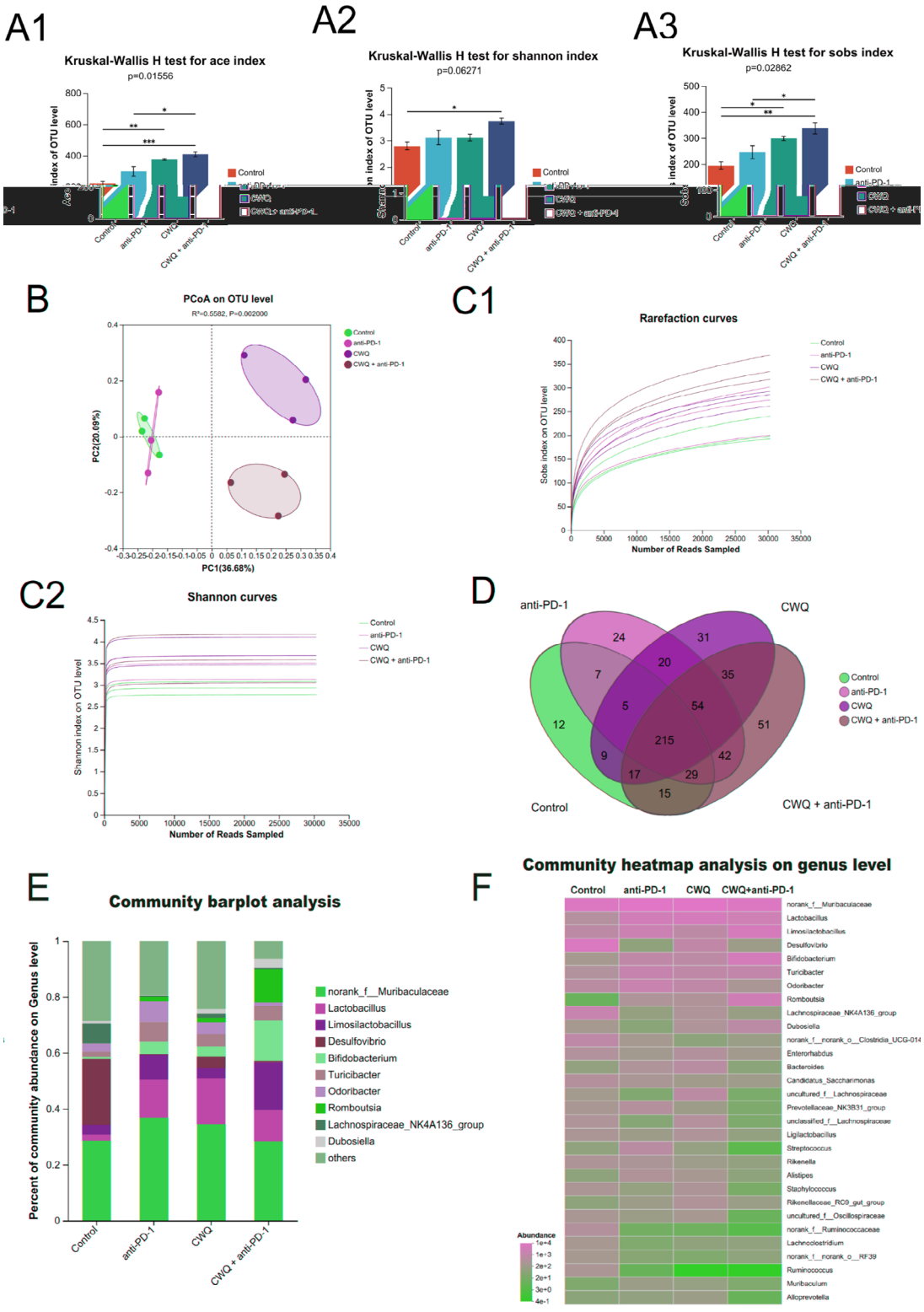

Fig. 3 CWQ combined with PD-1 inhibitor restores gut dysbiosis in CAC. (**A**) The ace index, shannon index, and sobs index show significant improvements in gut microbiota diversity with CWQ and PD-1 inhibitor. (**B**) PCoA reveals gut microbiota reshaping by CWQ combined with PD-1 inhibitor. (**C**) Rarefaction and shannon curves derived from the sobs index and shannon index. (**D**) OTU analysis reveals enhanced microbial diversity and abundance with CWQ combined with PD-1 inhibitor. (**E**) Community barplot analysis among different groups. (**F**) Community heatmap analysis on genus level among different groups. *$P < 0.05$, **$P < 0.01$ and ***$P < 0.001$

on microbial dysbiosis in CAC and contribute to the restoration of a healthy microbiota.

To investigate the potential role of gut microbiota and metabolites in mediating the chemopreventive effects of CWQ in conjunction with PD-1 inhibitor in CAC, fecal samples from the control group (FMT-Control), PD-1 inhibitor group (FMT-anti-PD-1), CWQ group (FMT-CWQ), and CWQ combined with PD-1 inhibitor treated mice (FMT-CWQ+anti-PD-1) were gavaged to AOM/DSS mice treated with antibiotic.

FMT-CWQ+anti-PD-1 significantly reduced DAI ($P<0.05$) (Fig. 4A), colon tumor number ($P<0.05$) (Fig. 4B) and maintained a higher weight in mice ($P<0.05$) compared to FMT-Control group (Fig. 4C). In FMT-Control mice, overlapping growth of tumors can be observed at the distal end of the rectum, with diameters mainly ranging from 2 to 4 millimeters, and some tumors also distributed within the intestine. In contrast, in the FMT-CWQ group, tumors are smaller, with only a few visible at the distal end of the rectum and exhibiting superficial growth. The number of tumors in FMT-anti-PD-1 mice is lower than in the FMT-Control group, yet tumors of varying sizes can still be observed at the distal end of the rectum. As for FMT-CWQ+anti-PD-1 mice, intestinal tumors are extremely rare, with only tiny tumor nodules appearing at the distal end of the rectum, and in some cases, no tumors are present (Fig. 4E). Following H&E staining of mouse colonic tissue slices, observations of the morphology of intestinal tissues from each group of mice were made using an optical microscope, and photographs were taken. In the FMT-Control group, the colonic mucosal structure appeared incomplete, with disrupted intestinal epithelial cells, accompanied by inflammatory cell infiltration, irregular mucosal layer hyperplasia, and loss of intestinal crypts. In the FMT-CWQ group, colonic cells were relatively intact, with visible crypts and numerous goblet cells, yet with some evidence of inflammatory cell infiltration. In the FMT-anti-PD-1 group mice, colonic mucosal structure was disrupted, showing evident villi fragmentation and atrophy, along with inflammatory cell infiltration, interstitial edema, and congestion, and a reduction in goblet cells. In the FMT-CWQ+anti-PD-1 group mice, the intestinal epithelial tissue appeared intact, with well-organized glands, no evidence of congestion or edema, and no inflammatory cell infiltration. (Fig. 4F). Through immunohistochemical analysis of Ki-67 expression in mice intestinal and tumor tissues (Fig. 4G), and utilizing Image J for analyzing the area of positive cell expression in histological sections, we observed that the expression of Ki-67 in FMT-CWQ group was downregulated compared to FMT-Control group ($P<0.01$). In FMT-CWQ+anti-PD-1 group, the expression level of Ki-67 exhibited a more pronounced downregulation trend compared to FMT-anti-PD-1 group ($P<0.001$). These data indicate that the anti-cancer effect of CWQ combined with PD-1 inhibitor is largely dependent on the gut microbiota.

CWQ Combined with PD-1 Inhibitor Modulates Gut Metabolites in CAC

Given the pivotal role of gut microbiota-derived metabolites in health and disease regulation, we proceeded with metabolic analysis on fecal samples from mice in the control group, CWQ group, PD-1 inhibitor group, and CWQ combined with PD-1 inhibitor group. Principal component analysis (PCA) and PLS-discriminant supervised analysis (PLS-DA) clearly demonstrated the distinct separation of metabolomes between the CWQ combined with PD-1 inhibitor and control groups in the CAC model (Fig. 5A and B). In the AOM/DSS models, 222 metabolites showed significant alterations in CWQ combined with PD-1 inhibitor-treated mice compared to control mice, with 174 being up-regulated and 48 down-regulated (Fig. 5C).

We utilized KEGG enrichment analysis to explore alterations in metabolic pathways and their biological implications by comparing the CWQ combined with PD-1 inhibitor group to the control group (Fig. 5D). The differential abundance score plot revealed that, compared to the control group, the CWQ combined with PD-1 inhibitor group exhibited varying degrees of modulation in immune system-related pathways (Fig. 5E). Importantly, the intervention of CWQ combined with PD-1 inhibitor led to the downregulation of most metabolites involved in *NF-kappa B signaling pathway*. In essence, this pathway was inhibited.

To link these metabolites with potential metabolic activities of gut microbes, we conducted integrative analyses of the altered microbiota and metabolites. Our findings revealed a negative correlation between the probiotic *Limosilactobacillus* and *LysoPC(18:1(11Z)/0:0)* ($P<0.01$) (Fig. 5F), while *Bifidobacterium* exhibited a negative correlation with *Avocadyne 4-acetate* ($P<0.001$). Conversely, the pathogenic bacteria *Desulfovibrio* was positively correlated with *LysoPC(16:0/0:0)* and *1-Palmitoylphosphatidylcholine* (all $P<0.05$). Collectively, the collaboration between metabolites and gut microbiota may contribute to enhancing the chemopreventive effects of CWQ combined with PD-1 inhibitor in CAC.

In our quest to unravel the molecular mechanisms underlying the tumor-suppressive properties of CWQ combined with PD-1 inhibitor in CAC, we delved into RNA sequencing of tumor tissues from two distinct CAC models. Our analysis revealed significant alterations, with 824 genes showing upregulation and 567 genes displaying downregulation in mice treated with CWQ combined with PD-1 inhibitor compared to the control group

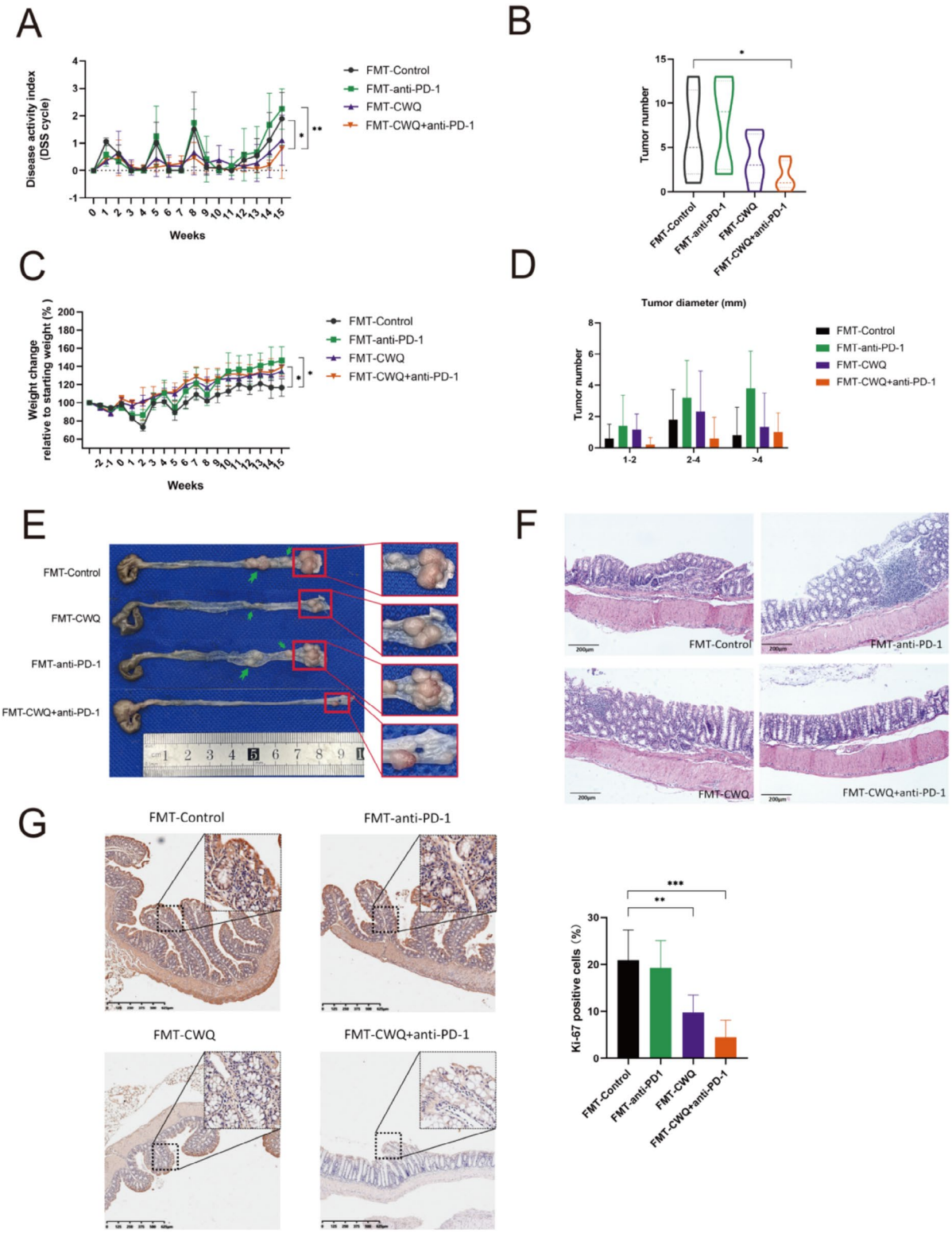

Fig. 4 CWQ combined with PD-1 inhibitor suppresses CAC in FMT model. (**A**) Changes in DAI of mice among different groups in the course of DSS cycle in FMT model. (**B**) Tumor numbers in mice subjected to different interventions within FMT model. (**C**) Body weight variations among different groups of mice within FMT model. (**D**) Tumor diameter in mice after different interventions within FMT model. (E) The features of colonic and tumor tissues of mice subjected to different interventions in FMT model. (**F**) H&E staining features of colonic mucosal tissues in mice following different interventions within FMT model. (**G**) Ki-67 expression in tumor tissues of mice following different interventions within FMT model. *$P < 0.05$, **$P < 0.01$ and ***$P < 0.001$

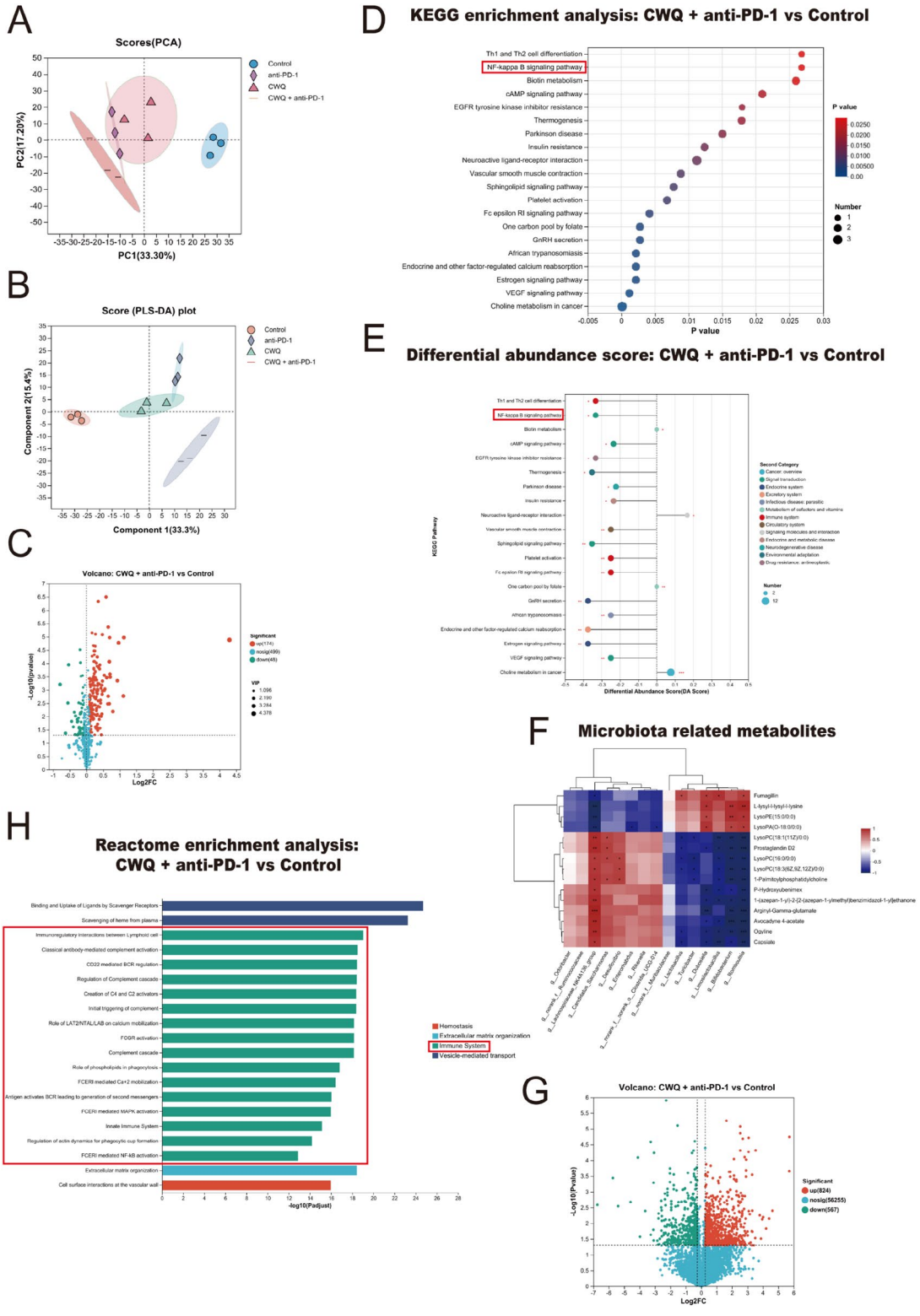

Fig. 5 CWQ combined with PD-1 inhibitor modulates gut metabolites in CAC. (**A**) PCA among different groups. (**B**) PLS-discriminant supervised analysis among different groups. (**C**) Differential metabolite volcano plot: CWQ combined with PD-1 inhibitor group compared to control group. (**D**) KEGG enrichment analysis of differential metabolites: CWQ combined with PD-1 inhibitor group compared to control group. (**E**) Differential abundance score plot of metabolites: CWQ combined with PD-1 inhibitor group compared to control group. (**F**) Integrative analyses of the altered microbiota and metabolites. (**G**) Differential gene volcano plot: CWQ combined with PD-1 inhibitor group compared to control group. (**H**) Reactome enrichment analysis of differential gene: CWQ combined with PD-1 inhibitor group compared to control group

(Fig. 5G). Further enrichment analysis using Reactome unveiled that these differentially expressed genes predominantly pertained to the immune system (Fig. 5H). This finding leads us to speculate that CWQ combined with PD-1 inhibitor may exert its effects by modulating the immune processes involved in CAC.

CWQ Combined with PD-1 Inhibitor Restores Intestinal Barrier Function in CAC

Gut dysbiosis stands as a pivotal factor contributing to the impairment of intestinal barrier function. To investigate the potential impact of CWQ combined with PD-1 inhibitor on the intestinal barrier, we examined variations in the states of intestinal tissues among different groups using TEM.

Under TEM, the control group displayed notable features, including swelling and localized discontinuity in the epithelial cells of the intestinal mucosa, as highlighted by the red circle. The microvilli (Mv) structure exhibited obscurity, disorganization, and local sparse or fused patterns, as indicated by the red arrows. Desmosomes (De) were scarce, intercellular spaces were narrow, and damage to the intestinal barrier structure was pronounced. In the submucosal tissue beneath the microvilli, a loose structure was observed. The mitochondria (M) were extensively damaged, characterized by fractured or disappearing mitochondrial cristae, visible electron-lucent areas, and some ruptured mitochondrial membranes, as indicated by the blue arrows. The endoplasmic reticulum showed a significant reduction in quantity, while the remaining endoplasmic reticulum exhibited conspicuous expansion. Ribosome numbers decreased, denoted by the yellow arrows, and autophagic bodies were evident, as indicated by the green arrows.

In contrast, mice treated with CWQ and PD-1 inhibitor exhibited relatively mild damage to intestinal mucosa epithelial cells. Their cell membranes remained intact, showcasing a more uniform cytoplasmic composition compared to the control group, and organelles displayed moderate swelling. Microvilli were more closely arranged, presenting a slender and uniform structure. Tight junctions (TJ) were present, with a short dense region and visible adherens junctions (AJ). The heightened abundance of desmosomes and the presence of narrow intercellular spaces indicated a mild disruption to the intestinal barrier. Mitochondria were abundant, featuring noticeable lipid droplets, mild swelling, intact membranes, partial matrix dissolution, and fractured or reduced mitochondrial cristae. Importantly, no typical autophagic structures were observed. Furthermore, in the CWQ combined with PD-1 inhibitor group, cell structures were dense, microvilli were orderly and notably elongated compared to other groups. Mitochondrial structure appeared relatively normal, exhibiting intact membranes and discernible mitochondrial granules, as indicated by purple arrows. The endoplasmic reticulum was more abundant, with no evident expansion observed (Fig. 6A).

To verify this conjecture, we first utilized immunohistochemistry to measure the levels of three proteins, ZO-1, Claudin, and Occludin, which are reliable markers for detecting the integrity of the intestinal barrier. The results demonstrated that, compared with the control group, CWQ combined with PD-1 inhibitor significantly restored the intestinal barrier function in two animal models (all $P<0.001$) (Fig. 6B and C). Subsequently, we synthesized two gene sets from the results of GO enrichment analysis and KEGG enrichment analysis, and then conducted GSEA (gene set enrichment analysis). Our investigations unveiled that the administration of CWQ combined with PD-1 inhibitor elicited an augmentation in the expression of genes associated with tight junctions and adherens junctions, concomitant with a reduction in genes linked to the innate immune response (Fig. 6D). Considering that most metabolites in the *NF-kappa B signaling pathway* are downregulated and the intestinal barrier function is repaired by CWQ combined with PD-1 inhibitor, these results indicate the potential of CWQ combined with PD-1 inhibitor in influencing related physiological conditions. This discovery not only reveals the value of this combination therapy within the scope of our current study but also guides us to further explore its broader implications in future research directions.

Discussion

In this investigation, the CWQ combined with PD-1 inhibitor demonstrated an anti-cancer effect in the AOM/DSS-induced CAC mouse model. Specifically, mice treated with the CWQ combined with PD-1 inhibitor showed a significant reduction in tumor number, smaller tumor sizes, and a more intact intestinal barrier. Dysbiosis of the gut microbiota can trigger immune responses in the host, leading to the development of inflammation and tumors. Using 16 S rRNA gene sequencing analysis, our study delved into the modulatory impact of CWQ combined with PD-1 inhibitor on the gut microbiota. The findings unveiled that this combination treatment not only enriched beneficial probiotics like *Limosilactobacillus* and *Bifidobacterium* but also inhibited pathogenic bacteria like *Desulfovibrio*, consequently reshaping the microbial composition and enhancing the richness and diversity of the gut microbiota. *Limosilactobacillus*, a prominent strain within the *Lactobacillus* genus, is notably recognized for its multifaceted capabilities, which include influencing gut flora, strengthening mucosal barriers, and producing bioactive compounds [23]. Specifically, *Limosilactobacillus* plays a pivotal role in immune regulation by adjusting cytokine expression and restoring

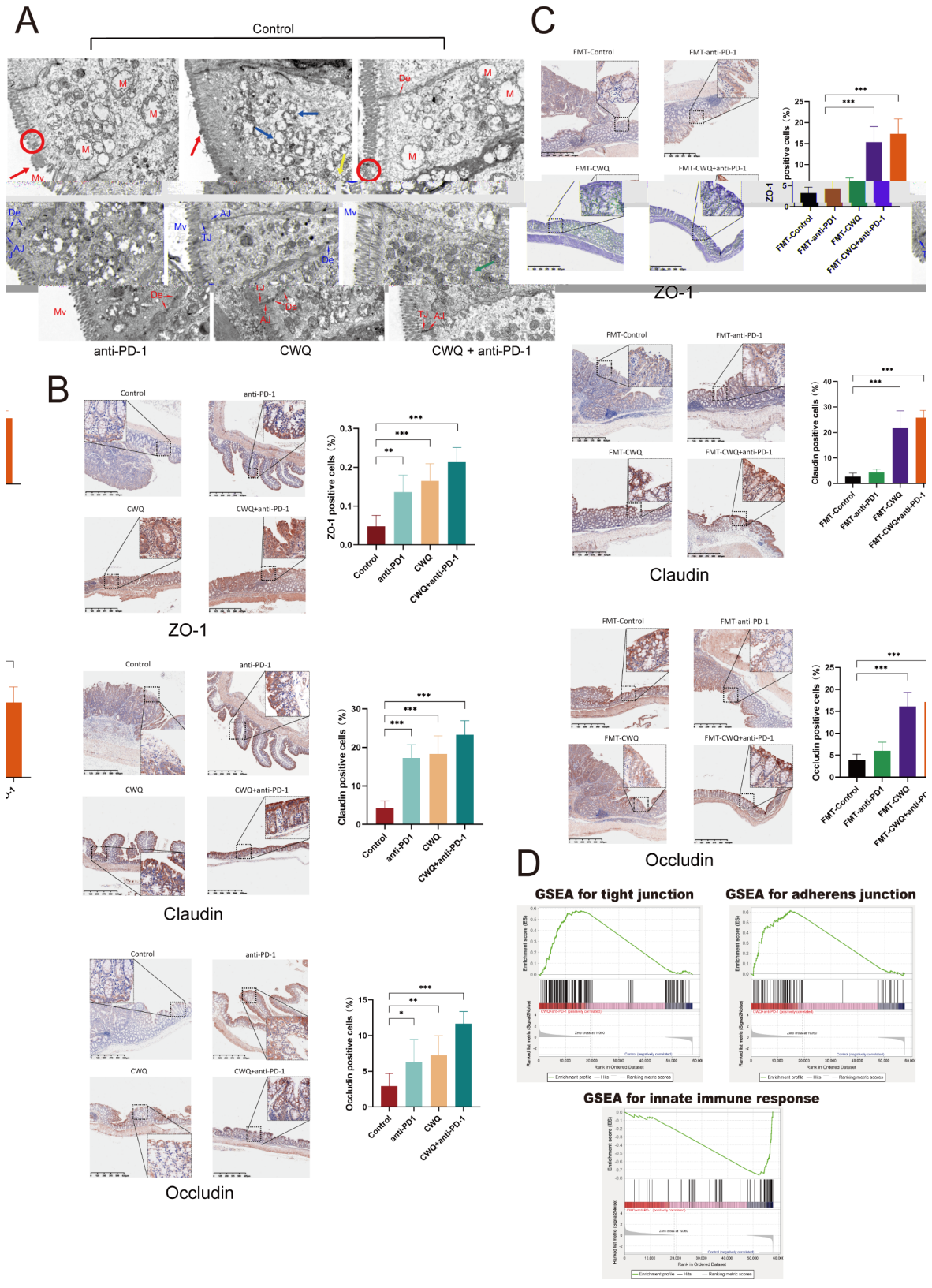

Fig. 6 CWQ combined with PD-1 inhibitor restores intestinal barrier function in CAC. (**A**) Variations in the state of intestinal organization in different groups under TEM. (**B**) The expression of ZO-1, Claudin, and Occludin in the intestinal tissues of mice after different interventions. (**C**) Expression profiles of ZO-1, Claudin, and Occludin in the intestinal tissues of mice following different interventions within FMT model. (**D**) GSEA of CWQ combined with PD-1 inhibitor group compared to control group. $^{*}P < 0.05$, $^{**}P < 0.01$ and $^{***}P < 0.001$

the Th1/Th2 balance [24]. Its strong adhesion to the gastrointestinal epithelial cell layer aids in maintaining and regulating barrier integrity and tightness [25], achieved through mechanisms such as mucin induction, tight junction maintenance, and anti-apoptotic effects. Moreover, *Limosilactobacillus* enhances the production of protective mucous layers, counters intestinal oxidative stress, and mitigates the harmful effects of intestinal pathogens by downregulating inflammatory mediators [24, 26]. On a different note, *Bifidobacterium* has demonstrated its ability to induce alterations in the fecal microbiota of CRC patients, concomitantly reducing specific cancer risk factors through enhanced epithelial barrier function and suppression of colorectal symbiotic microorganism proliferation [27]. Additionally, it showcases proficiency in reducing pro-inflammatory cytokines at both the gastrointestinal mucosal immune system and systemic immune system levels [28]. Conversely, the presence of *Desulfovibrio* poses risks of colonic injury and fosters a premetastatic milieu conducive to tumor metastasis, along with potential DNA damage and CRC progression due to H_2S production [22]. Various therapeutic approaches targeting *Desulfovibrio* suggest that probiotic treatment can effectively suppress *Desulfovibrio* abundance, leading to significant improvements in clinical outcomes. For example, oral administration of *Bifidobacterium* can reduce *Desulfovibrio* abundance, thereby improving colitis and CRC in rats [29]. Similarly, administering *Lactobacillus* can also reduce *Desulfovibrio* abundance, decrease AOM/DSS-induced CAC incidence, enhance tight junction protein expression, and reduce pro-inflammatory cytokine levels [30]. This microbial balance is crucial for bolstering the intestinal barrier's functionality and orchestrating immune responses within the host.

To probe further into the gut microbiota's role in inhibiting tumor development, this study conducted FMT experiments. Compared to the FMT-Control group, mice in FMT-CWQ+anti-PD-1 group exhibited a significant reduction in DAI, colon tumor number, and maintained colonic integrity. These findings indicate that the alteration of the gut microbiota induced by CWQ combined with PD-1 inhibitor contributes to its chemopreventive effect on CAC.

The intestinal barrier, consisting of a single layer of columnar epithelial cells, which selectively absorb nutrients while restricting the invasion of pathogens. Therefore, normal intestinal barrier function is essential for maintaining intestinal homeostasis. The inflammatory microenvironment and dysbiosis of gut microbiota can lead to intestinal mucosal damage and disrupt the structure of intercellular connections of intestinal epithelial cells, thereby impairing intestinal barrier function and intestinal homeostasis [31]. These changes can be observed as structural damage under TEM. In this study, the AOM/DSS-induced CAC mouse model exhibited significant disruption of the intestinal barrier structure, including epithelial cell swelling, microvilli disorganization, and extensive mitochondrial damage under TEM. In contrast, mice treated with CWQ and PD-1 inhibitor showed mild intestinal damage, with intact cell membranes, organized microvilli, and improved mitochondrial structure. Notably, the CWQ combined with PD-1 inhibitor group exhibited dense cell structures, elongated microvilli, and relatively normal mitochondria, indicating a protective effect on the intestinal barrier and, in turn, inhibiting the occurrence and progression of CAC.

Following this, the metabolic analysis revealed significant alterations in metabolites between the CWQ combined with PD-1 inhibitor group and the control group, indicating a distinct metabolic profile induced by the combination therapy. Specifically, KEGG enrichment analysis highlighted inflammation-related pathway that was notably downregulated in the CWQ combined with PD-1 inhibitor group compared to the control group. This suggests a reduction in inflammation levels following the combined treatment. These findings underscore the potential anti-inflammatory effects of CWQ combined with PD-1 inhibitor, which may contribute to its chemopreventive efficacy in CAC (Fig. 7).

Research indicates that proper immune responses play a vital role in pathogen clearance, benefiting the body. However, excessive immune responses can be detrimental. Inflammatory reactions often arise from intense immune activity. Normally, inflammation is self-limiting, but in tumors, it becomes persistent and challenging to control. Failure to resolve acute inflammation can progress to chronic inflammation, activating oncogenes, causing DNA and protein damage, reative oxygen species release, and impacting signaling pathways like *NF-kappa B*, leading to inflammation-to-cancer transition [32]. The intestinal tract, the body's largest mucosal surface, is constantly exposed to microbial and dietary influences. This heightened exposure renders the intestine more prone to both acute and chronic inflammation, a significant contributor to cancer development. Importantly, individuals experiencing chronic inflammation significantly elevate their risk of developing CRC [33]. *NF-kappa B*, as a core regulator of inflammatory response, plays a critical role in the pathogenesis of various inflammatory diseases. It stimulates the expression of pro-inflammatory cytokines, which contribute to tissue damage linked with inflammation [34]. Furthermore, *NF-kappa B* is involved in regulating tumor proliferation and survival. It induces the expression of genes involved in angiogenesis, affecting the development and metastasis of tumors [33]. In the intestine, the upregulation of *NF-kappa B* signaling promotes the progression of CAC, while probiotics inhibit *NF-kappa B* in intestinal epithelial cells, effectively

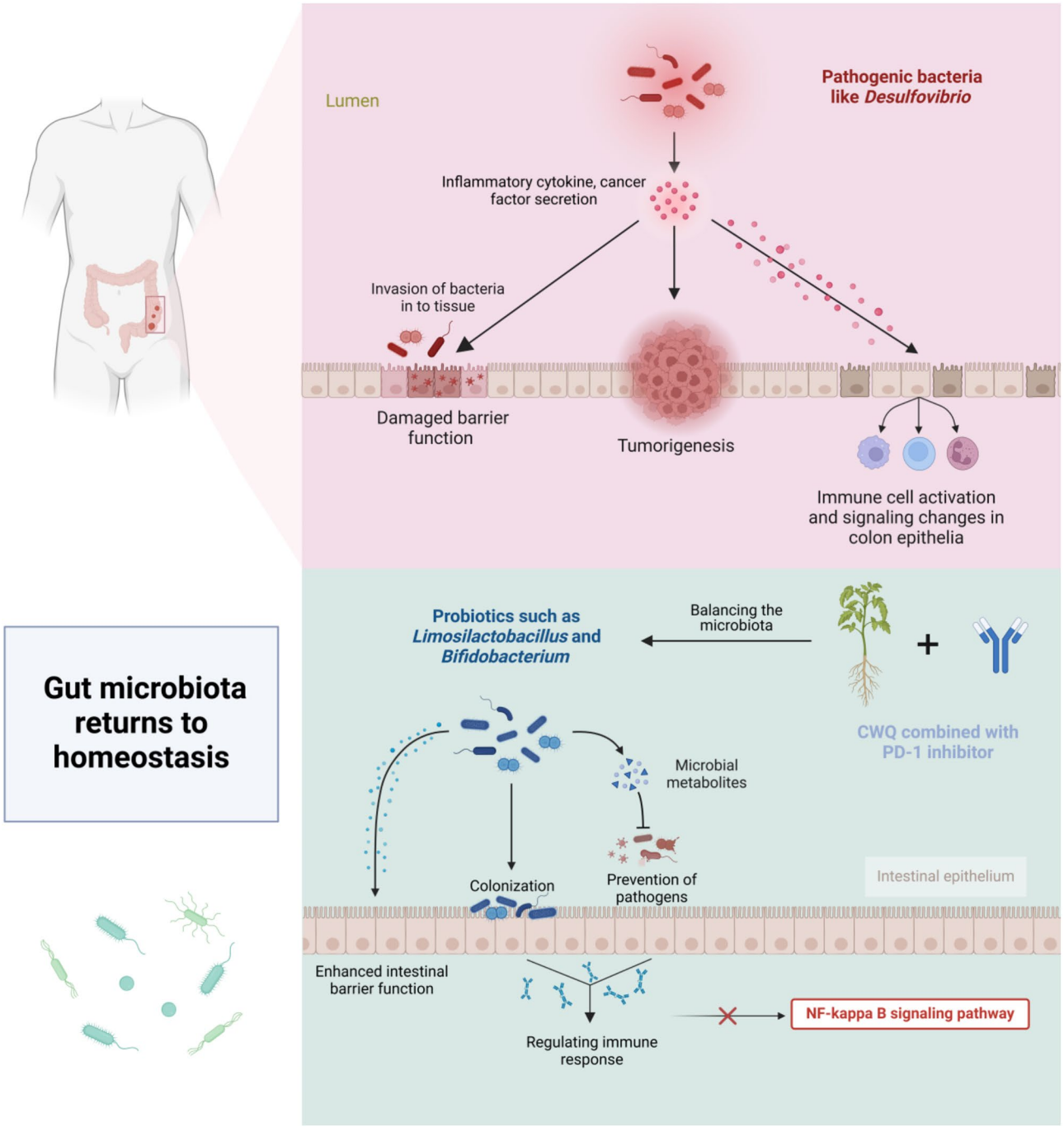

Fig. 7 Schematic diagram of the mechanism. Intestinal inflammation causes defects in the intestinal epithelial barrier, dysbiosis of microbial ecology, and excessive upregulation of immune responses. CWQ combined with PD-1 inhibitor improves dysbiosis in the AOM/DSS mouse model, thereby enhancing intestinal barrier function, ultimately restoring intestinal homeostasis and inhibiting CAC occurrence

preventing CAC in mice [35]. Excessive inflammatory response not only increases the burden of cancer but also severely disrupts the integrity of the intestinal barrier [36]. Given the close connection between inflammation and tumors, numerous studies have confirmed that controlling inflammation appears to be a more effective anti-cancer approach. Non-steroidal anti-inflammatory drugs, especially aspirin, have powerful chemopreventive effects. Similarly, statins significantly reduce the risk of various cancers by exerting anti-inflammatory effects [32].

Through the combined treatment of CWQ and PD-1 inhibitor, we modulate the gut microbiota in AOM/DSS-induced mice and improve intestinal barrier function.

There are indications of the potential to inhibit pro-inflammatory pathways, although this has not been proven in the current experiment. We will further study this aspect. Specifically, we aim to explore in depth the detailed molecular mechanisms underlying this potential anti-inflammatory effect, such as identifying the key downstream targets and the relevant signaling pathways. In addition, we plan to examine how this potential suppression of inflammation affects the overall progression of CAC using more complex in -vivo and in -vitro models. This will enable us to gain a more comprehensive understanding of the therapeutic potential of CWQ combined with PD-1 inhibitor in the treatment of CAC.

Conclusion

This research provides pioneering evidence concerning the anti-cancer efficacy of CWQ in combination with PD-1 inhibitor in mice induced by AOM/DSS. Furthermore, it has been discovered that the combined treatment augments the abundance of the intestinal microbiota. Specifically, it enriches probiotic bacteria including *Limosilactobacillus* and *Bifidobacterium*, while reducing the amount of pathogenic bacteria such as *Desulfovibrio*. Additionally, the metabolites of the gut microbiota might also possess anti-inflammatory activity. Moreover, CWQ combined with PD-1 restores the intestinal barrier. Therefore, CWQ combined with PD-1 inhibitor exerts its anti-CAC effect through modulating the gut microbiota, safeguarding the integrity of the intestinal barrier, and thus inhibiting the development of CAC.

Abbreviations

CWQ	Chang-Wei-Qing
CAC	Colitis-associated colorectal cancer
AOMt	Azoxymethane
DSS	Dextran sulfate sodium
CRC	Colorectal cancer
TCM	Traditional Chinese Medicine
FMT	Fecal microbiota transplantation
H&E	Hematoxylin-eosin
OUT	Operational taxonomic unit
DEGs	Differential expression genes
DAI	Disease activity index
PCoA	Principal coordinates analysis
PCA	Principal component analysis
PLS	DA-PLS-discriminant supervised analysis
TEM	Transmission electron microscopy
GSEA	Gene set enrichment analysis

Acknowledgements

We express our gratitude to the diligent efforts and valuable insights provided by the editors and reviewers. Additionally, we extend our appreciation to BioRender.com for the graphical resources employed in the illustrations.

Author Contributions

J.W. did writing - original draft, methodology, and formal analysis. S.W. did methodology, investigation and writing - review & editing. K.S. and H.W. did investigation and data curation. Z.Y. did supervision and conceptualization. W.D. did writing - review & editing, validation, supervision, resources, funding acquisition, and conceptualization. All authors reviewed the manuscript.

Funding

The work was funded by Shanghai Putuo District Health and Health System Science and Technology Innovation Project (No. ptkwws202002), Shanghai Putuo District Health and Health System Clinical Specialty Construction Project (No. 2021tszk01), Shanghai Municipal Health Commission's Shanghai Further Accelerating Traditional Chinese Medicine Development Three-Year Action Plan Project (No. ZY[2021–2023]-0302).

Data Availability

No datasets were generated or analysed during the current study.

Declarations

Ethics Approval and Consent to Participate

All animal experiments were approved by the Animal Experimentation Ethics Committee of Shanghai University of TCM and conducted by the Guide for the Care and Use of Laboratory Animals (approval number: DWEC-A-202206012).

Competing Interests

The authors declare no competing interests.

Author details

[1]Department of Oncology, Putuo Hospital, Shanghai University of Traditional Chinese Medicine, 164 Lanxi Road, Shanghai 200062, China
[2]Interventional Cancer Institute of Chinese Integrative Medicine, Putuo Hospital, Shanghai University of Traditional Chinese Medicine, 164 Lanxi Road, Shanghai 200062, China

Received: 20 September 2024 / Accepted: 5 December 2024
Published online: 19 December 2024

References

1. Sung H, Ferlay J, Siegel RL, Laversanne M, Soerjomataram I, Jemal A, et al. Global Cancer statistics 2020: GLOBOCAN estimates of incidence and Mortality Worldwide for 36 cancers in 185 countries. Cancer J Clin. 2021;71:209–49.
2. Morgan E, Arnold M, Gini A, Lorenzoni V, Cabasag CJ, Laversanne M et al. Global burden of colorectal cancer in 2020 and 2040: incidence and mortality estimates from GLOBOCAN. Gut [Internet]. 2022;72:gutjnl-2022-327736. https://gut.bmj.com/content/72/2/338
3. Li J, Ji Y, Chen N, Dai L, Deng H. Colitis-associated carcinogenesis: crosstalk between tumors, immune cells and gut microbiota. Cell Bioscience. 2023;13.
4. Lin K-H, Istl AC, Quan D, Skaro A, Tang E, Zheng X. PD-1 and PD-L1 inhibitors in cold colorectal cancer: challenges and strategies. Cancer Immunol Immunother. 2023;72:3875–93.
5. Sharma P, Goswami S, Raychaudhuri D, Siddiqui BA, Singh P, Nagarajan A, et al. Immune checkpoint therapy—current perspectives and future directions. Cell. 2023;186:1652–69.
6. Ramos-Casals M, Brahmer JR, Callahan MK, Flores-Chávez A, Keegan N, Khamashta MA et al. Immune-related adverse events of checkpoint inhibitors. Nature Reviews Disease Primers [Internet]. 2020 [cited 2021 Nov 24];6:1–21. https://www.nature.com/articles/s41572-020-0160-6?proof=t
7. Heregger R, Florian Huemer, Steiner M, Gonzalez-Martinez A, Greil R, Weiss L. Unraveling resistance to Immunotherapy in MSI-High Colorectal Cancer. Cancers. 2023;15:5090–0.
8. Yu LC-H. Microbiota dysbiosis and barrier dysfunction in inflammatory bowel disease and colorectal cancers: exploring a common ground hypothesis. Journal of Biomedical Science [Internet]. 2018 [cited 2020 Jan 20];25. https://jbiomedsci.biomedcentral.com/articles/https://doi.org/10.1186/s12929-018-0483-8
9. Lichtenstern CR, Ngu RK, Shalapour S, Karin M. Immunotherapy, inflammation and colorectal Cancer. Cells. 2020;9:618.
10. Lu Y, Yuan X, Wang M, He Z, Li H, Wang J et al. Gut microbiota influence immunotherapy responses: mechanisms and therapeutic strategies. J Hematol Oncol. 2022;15.
11. Brennan CA, Garrett WS. Gut Microbiota, Inflammation, and Colorectal Cancer. Annual review of microbiology [Internet]. 2016 [cited 2020 Apr 28];70:395–411. https://www.ncbi.nlm.nih.gov/pmc/articles/PMC5541233/

12. Chen Y, Liu B, Wei Y, Kuang D-M. Influence of gut and intratumoral microbiota on the immune microenvironment and anti-cancer therapy. Pharmacol Res. 2021;174:105966–6.
13. Hiraishi K, Zhao F, Kurahara L-H, Li X, Yamashita T, Hashimoto T, et al. Lactulose modulates the structure of Gut Microbiota and Alleviates Colitis-Associated Tumorigenesis. Nutrients. 2022;14:649.
14. Zhao Y, Jiang Q. Roles of the polyphenol–gut Microbiota Interaction in Alleviating Colitis and Preventing Colitis-Associated Colorectal Cancer. Adv Nutr. 2020;12:546–65.
15. Feng W, Ao H, Peng C, Yan D. Gut microbiota, a new frontier to understand traditional Chinese medicines. Pharmacol Res. 2019;142:176–91.
16. Lin T-L, Lu C-C, Lai W-F, Wu T-S, Lu J-J, Chen Y-M, et al. Role of gut microbiota in identification of novel TCM-derived active metabolites. Protein Cell. 2020;12:394–410.
17. Wang T, Wu L, Wang S, Shi X, Liu H, Deng W. Chang Wei Qing Decoction enhances the anti-tumor effect of PD-1 inhibitor therapy by regulating the immune microenvironment and gut microbiota in colorectal cancer. Chinese Journal of Natural Medicines [Internet]. 2023 [cited 2023 Nov 1];21:333–45. https://www.sciencedirect.com/science/article/pii/S1875536423604510
18. Wang L, Wang R, Wei G, Wang S, Du G. Dihydrotanshinone attenuates chemotherapy-induced intestinal mucositis and alters fecal microbiota in mice. Biomed Pharmacother. 2020;128:110262–2.
19. Kim S, Hwan H, Lee, Kang C-H, Kang H, Cho H. Immune-Enhancing effects of Limosilactobacillus fermentum in BALB/c mice immunosuppressed by Cyclophosphamide. Nutrients. 2023;15:1038–8.
20. Mills S, Yang B, Smith GJ, Stanton C, Ross RP. Efficacy of Bifidobacterium longum alone or in multi-strain probiotic formulations during early life and beyond. Gut Microbes. 2023;15.
21. Azad MAK, Sarker M, Li T, Yin J. Probiotic Species in the Modulation of Gut Microbiota: An Overview. BioMed Research International [Internet]. 2018;2018:1–8. https://www.ncbi.nlm.nih.gov/pmc/articles/PMC5964481/
22. Singh SB, Carroll-Portillo A, Lin HC. Desulfovibrio in the Gut: The Enemy within? Microorganisms [Internet]. 2023 [cited 2023 Oct 23];11:1772. https://www.mdpi.com/2076-2607/11/7/1772
23. Kubota M, Ito K, Tomimoto K, Kanazaki M, Tsukiyama K, Kubota A, et al. Lactobacillus reuteri DSM 17938 and Magnesium Oxide in children with functional chronic constipation: a double-blind and randomized clinical trial. Nutrients. 2020;12:225.
24. Un-Nisa A, Khan A, Zakria M, Siraj S, Ullah S, Tipu MK, et al. Updates on the role of probiotics against different Health issues: focus on Lactobacillus. Int J Mol Sci. 2022;24:142.
25. Schlee M, Harder J, Köten B, Stange EF, Wehkamp J, Fellermann K. Probiotic lactobacilli and VSL#3 induce enterocyte β-defensin 2. Clin Experimental Immunol. 2008;151:528–35.
26. Cordeiro L, Diego C, Lacerda DS, Ferreira, Leite E, Luiz J. Limosilactobacillus Fermentum, current evidence on the antioxidant properties and opportunities to be exploited as a probiotic microorganism. Probiotics Antimicrob Proteins. 2022;14:960–79.
27. Hidalgo-Cantabrana C, Delgado S, Ruiz L, Ruas-Madiedo P, Sánchez B, Margolles A. Bifidobacteria and Their Health-Promoting Effects. Bugs as Drugs [Internet]. 2018;5:73–98. https://www.asmscience.org/content/journal/microbiolspec/https://doi.org/10.1128/microbiolspec.BAD-0010-2016
28. Groeger D, O'Mahony L, Murphy EF, Bourke JF, Dinan TG, Kiely B et al. Bifidobacterium infantis 35624 modulates host inflammatory processes beyond the gut. Gut Microbes [Internet]. 2013;4:325–39. https://pubmed.ncbi.nlm.nih.gov/23842110/
29. Bi Z, Cui E, Yao Y, Chang X, Wang X, Zhang Y et al. Recombinant Bifidobacterium longum carrying endostatin protein alleviates Dextran Sodium Sulfate-Induced colitis and Colon cancer in rats. Front Microbiol. 2022;13.
30. Wang T, Zhang L, Wang P, Liu Y, Wang G, Shan Y, et al. Lactobacillus coryniformis MXJ32 administration ameliorates azoxymethane/dextran sulfate sodium-induced colitis-associated colorectal cancer via reshaping intestinal microenvironment and alleviating inflammatory response. Eur J Nutr. 2021;61:85–99.
31. Luissint A-C, Parkos CA, Nusrat A. Inflammation and the Intestinal Barrier: Leukocyte–Epithelial Cell Interactions, Cell Junction Remodeling, and Mucosal Repair. Gastroenterology [Internet]. 2016 [cited 2019 Oct 31];151:616–32. https://www.ncbi.nlm.nih.gov/pmc/articles/PMC5317033/
32. Zhao H, Wu L, Yan G, Chen Y, Zhou M, Wu Y et al. Inflammation and tumor progression: signaling pathways and targeted intervention. Signal Transduct Target Therapy. 2021;6.
33. Hirano T, Hirayama D, Wagatsuma K, Yamakawa T, Yokoyama Y, Nakase H. Immunological mechanisms in inflammation-Associated Colon carcinogenesis. Int J Mol Sci. 2020;21:3062.
34. O'Connor PM, Lapointe TK, Beck PL, Buret AG. Mechanisms by which inflammation may increase intestinal cancer risk in inflammatory bowel disease. Inflamm Bowel Dis. 2010;16:1411–20.
35. Xiao H, Gulen MF, Qin J, Yao J, Bulek K, Kish D, et al. The toll–Interleukin-1 receptor Member SIGIRR regulates colonic epithelial homeostasis, inflammation, and Tumorigenesis. Immunity. 2007;26:461–75.
36. Chen Y, Cui W, Li X, Yang H. Interaction between commensal Bacteria, Immune Response and the Intestinal Barrier in Inflammatory Bowel Disease. Front Immunol. 2021;12.

Publisher's Note